The role of accelerated growth plate fusion in the absence of SOCS2 on osteoarthritis vulnerability

Hasmik J. Samvelyan[1,2], Carmen Huesa[3], Lucy Cui Lin[4], Colin Farquharson[4], Katherine A. Staines[1,2*]

[1]School of Pharmacy and Biomolecular Sciences, University of Brighton, Brighton UK

[2] Centre for Stress and Age-Related Disease, University of Brighton, Brighton, UK

[3]Institute of Infection, Immunity & Inflammation, College of Medical, Veterinary and Life Sciences, University of Glasgow

[4]The Roslin Institute, The University of Edinburgh, Edinburgh, UK

Corresponding author

Katherine Ann Staines, University of Brighton, Lewes Road, Brighton BN2 4GJ

Email: k.staines@brighton.ac.uk Tel: 01273 642 094

ORCID ID: 0000-0002-8492-9778

Key words: osteoarthritis; SOCS2; cartilage; growth plate; bone; growth hormone

Summary statement: Deletion of SOCS2 results in accelerated growth plate fusion, however this has no effect on osteoarthritis vulnerability.

Abstract

Osteoarthritis is the most prevalent systemic musculoskeletal disorder characterised by articular cartilage degeneration and subchondral bone (SCB) sclerosis. Here we sought to examine the contribution of accelerated growth to osteoarthritis development using a murine model of excessive longitudinal growth. Suppressor of cytokine signalling 2 (SOCS2) is a negative regulator of growth hormone (GH) signalling, thus mice deficient in SOCS2 (*Socs2*$^{-/-}$) display accelerated bone growth. We examined vulnerability of *Socs2*$^{-/-}$ mice to osteoarthritis following surgical induction of disease (destabilisation of the medial meniscus (DMM)), and with ageing, by histology and micro-CT. We observed significant increase in number (WT DMM: 532±56; WT sham: 495±45; KO DMM: 169±49; KO sham: 187±56; P<0.01) and density (WT DMM: 2.2±0.9; WT sham: 1.2±0.5; KO DMM: 13.0±0.5; KO sham: 14.4±0.7) of growth plate bridges in *Socs2*$^{-/-}$ in comparison to wild-type (WT). Histological examination of WT and *Socs2*$^{-/-}$ knees revealed articular cartilage damage with DMM in comparison to sham (WT DMM: 3.4±0.4; WT sham: 0.3±0.05 (P<0.05); KO DMM: 3.2±0.8; KO sham: 0.8±0.3). Articular cartilage lesion severity scores (mean and maximum) were similar in WT and *Socs2*$^{-/-}$ mice with either DMM, or with ageing. Micro-CT analysis revealed significant decreases in SCB thickness, epiphyseal trabecular number and thickness in the medial compartment of *Socs2*$^{-/-}$, in comparison to WT (P<0.001). DMM had no effect on the SCB thickness in comparison to sham in either genotype. Together these data suggest that enhanced GH signalling through SOCS2 deletion accelerates growth plate fusion, however this has no effect on osteoarthritis vulnerability in this model.

Introduction

Osteoarthritis is the most prevalent systemic musculoskeletal disorder characterised by degeneration of joint articular cartilage, osteophyte formation, subchondral bone plate thickening, synovial proliferation and inflammation. Osteoarthritis has a multifactorial aetiology including ageing, trauma, obesity and heredity. Further, a complex interplay of major molecules and signalling pathways play indispensable roles in osteoarthritis development (Chang et al., 2019; Echtermeyer et al., 2009; Glasson et al., 2005; Saito et al., 2010; Wang et al., 2013). Despite this, effective disease-modifying treatments are currently limited.

Endochondral ossification is an essential process for longitudinal bone growth. It requires hypertrophic differentiation of chondrocytes characterised by secretion of type X collagen (COL10A1), matrix metalloproteinase-13 (MMP-13) and vascular endothelial growth factor (VEGF), followed by the subsequent degradation and conversion of the cartilage matrix into highly vascularised bone tissue (Kronenberg, 2003; Nagao et al., 2017). Osteoarthritis is widely accepted to involve the reversion of chondrocyte behaviour to an earlier developmental-like phenotype, which could drive the disease process. Indeed, re-expression of the type IIA procollagen, a spliced variant of the type II collagen gene (COL2A1) normally expressed in chondroprogenitor cells, in adult osteoarthritic articular chondrocytes indicates reversion of these cells to early developmental-like phenotype (Aigner et al., 1999).

Consistent with this, we have previously shown the abnormal deployment of a transient chondrocyte phenotype in the joints of a STR/ort mouse (Staines et al., 2016), a murine model for spontaneous osteoarthritis (Samvelyan et al., 2020). Further, we revealed accelerated long bone growth, a wider zone of growth plate proliferative chondrocytes, and widespread COL10A1 and MMP-13 expression beyond the expected hypertrophic zone distribution in these mice, which may underpin their osteoarthritis onset (Staines et al., 2016).

However, the precise contribution of accelerated growth to osteoarthritis development remains unclear.

Suppressor of cytokine signalling 2 (SOCS2), one of the members of the suppressor of cytokine signalling family glycoproteins, is implicated in cancer and disorders of immune system and central nervous system (Cramer et al., 2019; Keating and Nicholson, 2019; Letellier and Haan, 2016). SOCS2 has been shown as a primary intracellular suppressor of growth hormone signalling pathway, thus mice deficient in SOCS2 (*Socs2*$^{-/-}$) display an excessive growth phenotype (Metcalf et al., 2000). Here we use this mouse model of accelerated bone growth to understand the association between aberrant growth dynamics and osteoarthritis development. To achieve this, we examined the vulnerability of *Socs2*$^{-/-}$ mice to osteoarthritis following surgical induction of disease (destabilisation of the medial meniscus (DMM)), and with ageing, by histology and micro computed tomography (micro-CT).

Results

Socs2$^{-/-}$ *mice exhibit accelerated growth plate fusion*

In accordance with the known effects of increased growth hormone (GH) signalling on the skeleton, we observed a significant increase in *Socs2*$^{-/-}$ body weight in comparison to WT controls in ageing (Socs2$^{-/-}$ 51.9g ± 1.4; WT 32.0g ± 0.5g; P<0.001), and throughout the 8-week DMM experiment (Table 1; P<0.001). We next sought to examine growth plate fusion in these mice. We observed a significant increase in the number of growth plate bridges in *Socs2*$^{-/-}$ mice in comparison to WT mice at both ages examined (Fig. 1). Specifically, we saw a significant increase in growth plate bridge number (Fig. 1A & B; WT DMM: 532 ± 56; WT sham: 495 ± 45; KO DMM: 169 ± 49; KO sham: 187 ± 56; P<0.01) and density (Fig. 1A & C; (WT DMM: 2.2 ± 0.9; WT sham: 1.2 ± 0.5; KO DMM: 13.0 ± 0.5; KO sham: 14.4 ± 0.7; P<0.01) in *Socs2*$^{-/-}$ sham and DMM tibiae (16 weeks of age), in comparison to WT sham and DMM tibiae (P<0.01). No differences in growth plate bridges

were observed with osteoarthritis intervention in either genotype. Concurrent with this, in aged mice (around 1 year), a significant increase in growth plate bridge number (Fig. 1D & E) and density (Fig. 1D & F) was observed in *Socs2*$^{-/-}$ mice in comparison to WT mice (WT: 585 ± 70; KO: 1659 ± 91; densities – WT: 8.6 ± 2.2; KO: 21.3 ± 1.4 P<0.001).

Socs2 deletion does not exacerbate the development of osteoarthritis in a DMM model

Assessment of cartilage damage in the medial tibia of WT mice revealed an increased articular cartilage OARSI score with DMM in comparison to sham (P<0.05; Fig. 2A, C & D). However, no significant differences in the articular cartilage mean and maximum OARSI severity scores were observed between WT and *Socs2*$^{-/-}$ mice (Fig. 2C & 2D). Similarly, whilst osteophytes were observed in both WT and *Socs2*$^{-/-}$ DMM mice, there was no difference between genotypes (Fig. 2B). Micro-CT analysis of the subchondral bone plate revealed a significantly thinner subchondral bone plate in the medial compartment of *Socs2*$^{-/-}$ knee joints, in comparison to WT knee joints (Fig. 3A; SCB Th. WT: 0.15mm ± 0.003; KO: 0.11mm ± 0.003; P<0.001). DMM had no effect on the subchondral bone plate thickness in comparison to sham in either WT or Socs2$^{-/-}$ knee joints (Fig. 3A). Similarly, no differences were observed in the subchondral bone % BV/TV between genotypes or osteoarthritis interventions (Fig. 3B). Micro-CT analysis of the epiphyseal trabecular bone also revealed no effect of DMM on % BV/TV (Fig. 3C), however we observed decrease in trabecular number (Fig. 3D; Tb. N. WT: 12.3mm^{-1} ± 0.2; KO: 10.6mm^{-1} ± 0.2; P<0.001) and increase in trabecular thickness (Fig. 3E; Tb. Th. WT: 0.06mm ± 0.001; KO: 0.07mm ± 0.002; P<0.05) in *Socs2*$^{-/-}$ knee joints in comparison to WT knee joints. DMM had no effect on the epiphyseal bone parameters in comparison to sham in either WT or *Socs2*$^{-/-}$ knee joints (Fig. 3C - F).

Socs2 deletion has no effect on joint ageing

To examine the effects of *Socs2* deletion in aged joints, histological examination revealed no differences in the articular cartilage lesion mean and maximum severity scores between aged WT and Socs2$^{-/-}$ mice in any of the joint compartments (Figs. 4A, B & 4C). Similar to our previous analysis of DMM treated WT and *Socs2*$^{-/-}$ mice (Fig. 3), micro-CT analysis of the subchondral bone revealed thinner subchondral bone plate in the medial compartment of *Socs2*$^{-/-}$ knee joints, in comparison to WT knee joints (Fig. 5A; SCB Th. WT: 0.2mm ± 0.005; KO: 0.1mm ± 0.004; P<0.001). No differences were observed in the subchondral bone % BV/TV between genotypes (Fig. 5B), however the epiphyseal trabecular BV/TV was decreased in *Socs2*$^{-/-}$ knee joints (Fig. 5C; Tb. BV/TV WT: 73.5% ± 1.5; KO: 64.6% ± 2.2; P<0.01). No significant differences were observed in trabecular number (Fig. 5D), trabecular thickness (Fig. 5E) or trabecular separation (Fig. 5F) between aged WT and Socs2$^{-/-}$ mice.

Discussion

Here we sought to examine whether altered growth plate dynamics underpin osteoarthritis through examination of osteoarthritis vulnerability in a murine model of accelerated growth (*Socs2*$^{-/-}$). We describe accelerated growth plate fusion in these mice, consistent with their known overgrowth phenotype. However, we found no effect of a surgical intervention or ageing on the articular cartilage or subchondral bone phenotype in these mice. This suggests that in this murine model, aberrant growth dynamics are not associated with vulnerability to osteoarthritis development.

It is well established that in osteoarthritis, chondrocytes in the articular cartilage adopt a more transient phenotype, similar to that seen in the growth plate (Pitsillides and Beier, 2011). This raises the question as to whether a greater understanding of the discordant chondrocyte phenotypes may inform on mechanisms underpinning osteoarthritis, and strategies for treatment. Our previous work has shown that in a spontaneous model of osteoarthritis (STR/Ort mouse), there is an association between aberrant growth plate dynamics and

147 osteoarthritis development (Staines et al., 2016). Specifically, we revealed STR/Ort mice
148 show an overgrowth phenotype with enriched growth plate bridging, which was associated
149 with articular cartilage lesions at 18-20 weeks of age (Staines et al., 2016). Further, our
150 previous work on the MRC National Survey of Health and Development revealed modest
151 associations between greater gains in height in childhood, indicative of accelerated growth,
152 and decreased odds of knee osteoarthritis at 53 years (Staines et al., 2020). Together this
153 suggests that the growth rate may play a role in the development of osteoarthritis, although
154 what that role is has yet to be fully defined.

155 SOCS2 is a negative regulator of GH signalling, via inhibition of the Janus kinase/signal
156 transducers and activators of transcription (JAK/STAT) pathway (Pass et al., 2009). Thus,
157 mice deficient in *Socs2*$^{-/-}$ display an excessive growth phenotype (Metcalf et al., 2000).
158 Characterisation of their growth phenotype has revealed increased bone growth rates, growth
159 plate widths, and chondrocyte proliferation in *Socs2*$^{-/-}$ 6□week□old mice compared to age-
160 matched wild-type mice (Pass et al., 2012). *Socs2*$^{-/-}$ mice have normal serum levels of GH
161 and insulin-like growth factor -1 (IGF-1), and their longitudinal growth phenotype is due to
162 local effects of the GH/IGF-1 axis on the growth plate (Macrae et al., 2009). Consistent with
163 this, we revealed increased numbers and densities of growth plate bridges in *Socs2*$^{-/-}$ mice, in
164 comparison to WT mice. Growth plate bridges form as the growth slows and undergoes
165 progressive narrowing. They are also known to form upon growth plate injury, thought to be
166 through an intramembranous ossification mechanism (Xian et al., 2004). However, whether
167 growth plate fusion occurs prior to or after the cessation of growth is of significant
168 controversy in the field and has been somewhat overlooked (Parfitt, 2002).

169 We have previously shown using finite element modelling growth plate bridging to increase
170 stress dissipation in the subchondral bone region of the joint (Madi et al., 2019; Staines et al.,
171 2018). It is therefore surprising that the increased growth plate bridging observed in our

172 *Socs2*$^{-/-}$ mice here had reduced subchondral bone plate and trabecular parameters. Previous
173 studies have examined the *Socs2*$^{-/-}$ bone phenotype with contradictory results. Our previous
174 work has shown that *Socs2*$^{-/-}$ mice have increased bone mass, trabecular number and
175 trabecular thickness (Dobie et al., 2018; Macrae et al., 2009). However, others have shown
176 the absence of SOCS2 to induce losses in cortical and trabecular bone mineral density
177 (Lorentzon et al., 2005). These results are not consistent with the expected augmented
178 GH/IGF-1 axis, but are consistent with our findings here and highlight the complexity of this
179 pathway and the need for further studies to elucidate the precise role of SOCS2 signalling in
180 bone homeostasis.

181 Increased GH but reduced IGF-1 concentrations are present in synovial fluid of patients with
182 osteoarthritis (Denko et al., 1996). However, in rodents deficiency of GH and IGF-1 causes
183 an increased severity of osteoarthritic articular cartilage lesions (Ekenstedt et al., 2006).
184 Further, it has previously been shown that *Socs2* mRNA levels are decreased in chondrocytes
185 from osteoarthritic femoral heads (de Andres et al., 2011). Together these data suggest a role
186 for the GH/IGF-1/SOCS2 pathway in the pathology of osteoarthritis. However, our results
187 presented here indicate that there is no effect of SOCS2 deficiency on osteoarthritis
188 vulnerability, and thus highlighting the need to better understand GH/IGF-1 signalling in the
189 aetiology of osteoarthritis. This may be due to the normal serum levels of GH/IGF-1
190 observed in *Socs2*$^{-/-}$ mice (Macrae et al., 2009).

191 Together, our data show that deletion of SOCS2 leads to accelerated growth plate fusion, but
192 this has no effect on osteoarthritis vulnerability in a surgical model of osteoarthritis. Future
193 studies will determine whether this lack of vulnerability is specific to this model of
194 accelerated longitudinal growth, or whether this is characteristic of osteoarthritis in general.

195 **Methods**

196 *Animals*

197 *Socs2*$^{\square/\square}$ mice on a C57/BL6 genetic background were generated as previously described
198 (Dobie et al., 2018). For genotyping, tail biopsied DNA was analysed by PCR for *Socs2* WT
199 (Forward: TGTTTGACTGAGCTCGCGC, Reverse: CAACTTTAGTGTCTTGGATCT) or
200 the neocassette (*Socs2* $^{-/-}$; Forward: ACCCTGCACACTCTCGTTTTG, Reverse:
201 CCTCGACTAAACACATGTAAAGC). Mice were kept in polypropylene cages, with
202 light/dark 12-h cycles, at 21 ± 2°C, and fed *ad libitum* with maintenance diet (Special Diet
203 Services, Witham, UK). Ageing studies were completed in 12-13-month-old *Socs2*$^{\square/\square}$ (n=6)
204 and C57/BL6 wild-type (WT; n=6) male mice (Charles River). Analyses were conducted
205 blindly to minimise the effects of subjective bias. All experimental protocols were approved
206 by Roslin Institute's Animal Users Committee and the animals were maintained in
207 accordance with UK Home Office guidelines for the care and use of laboratory animals.

208 *Destabilisation of the medial meniscus (DMM)*

209 Osteoarthritis was induced in 8-week old *Socs2*$^{\square/\square}$ (n=6) and C57/BL6 WT (n=6) male mice
210 (Charles River) by surgically induced DMM under isoflurane-induced anaesthesia. Following
211 transection of the medial meniscotibial ligament to destabilise the medial meniscus, the left
212 knee joint capsule and skin were closed and anaesthesia reversed. Sham□operated joints
213 were used as controls. After 8 weeks, knee joints were dissected, fixed in 4%
214 paraformaldehyde for 24 hours at 4^{o}C, and then stored in 70% ethanol.

215 *Micro-CT analysis*

216 Scans of the right knee joint were performed with an 1172 X-Ray microtomograph (Skyscan,
217 Belgium) to evaluate the subchondral bone. High-resolution scans with voxel size of 5 µm
218 were acquired (50 kV, 200µA, 0.5 mm aluminium filter, 0.6° rotation angle). The projection
219 images were reconstructed using NRecon software version 1.6.9.4 (Skyscan, Belgium). Each
220 dataset was rotated in DataViewer (Skysan, Belgium) to ensure similar orientation and
221 alignment for analysis. Hand-drawn regions of interests (ROI) of the subchondral trabecular

bone for each femur and tibia lateral/medial compartments was first achieved. Subchondral bone ROIs was subsequently selected for each compartment. Analysis of subchondral bone plate thickness and the epiphyseal trabecular bone was achieved using 3D algorithms in CTAn (Skyscan, Belgium) to provide: subchondral bone plate thickness (SCB Th.; mm); subchondral bone plate bone volume/tissue volume (SCB BV/TV; %); epiphyseal trabecular bone volume/tissue volume (Tb. BV/TV; %); trabecular number (Tb. N.; mm^{-1}); trabecular thickness (Tb. Th.; mm) and trabecular separation (Tb. Sp.; mm).

Growth plate bridging analysis

Growth plate bridging analysis was conducted using a 3D micro-CT quantification method as previously described (Madi et al., 2019; Staines et al., 2018). Briefly, micro-CT scans of the tibiae were segmented using a region-growing algorithm within the Avizo® (V8.0, VSG, Burlington, VT, USA) software. The central points of all bony bridges were identified and projected on the tibial joint surface. The distribution of the areal number density of bridges (N, the number of bridges per 256 µm × 256 µm window) is then calculated and superimposed on the tibial joint surface (each bridge has a colour that represents the areal number density at the bridge location).

Histological analysis

Murine left knee joints were decalcified, wax-embedded and 6µm coronal sections cut. For assessment of osteoarthritis severity, multiple sections (>5/slide) from 120µm intervals across the whole joint were stained with Toluidine blue (0.4% in 0.1 M acetate buffer, pH 4). Articular cartilage damage was assessed in the medial tibia using the well-established OARSI grading scale, with scores averaged (Glasson et al., 2010). Osteophytes were also scored where 0 = none; 1 = formation of cartilage-like tissue; 2 = increase in cartilaginous matrix; 3 = endochondral ossification (Nagira et al., 2020). Scoring was conducted blindly with by two observers.

Statistical analysis

All analyses were performed with GraphPad Prism software 6.0f version (GraphPad Inc, La Jolla, CA, USA). The results were presented as the mean ± standard error of the mean (SEM). Normal distribution of data was assessed using the Shapiro-Wilk normality test. For the growth plate bridging and micro-CT analysis, two-way ANOVA with Bonferroni adjustments for multiple comparisons were used. For articular cartilage damage, the Kruskal-Wallis one-way ANOVA was used for DMM studies, and the Mann-Whitney U test for ageing studies. The significance was set at $P<0.05$.

Acknowledgements

The authors would like to thank Dr Blandine Poulet of University of Liverpool, Institute of Ageing and Chronic Disease for her guidance in experimental techniques and insightful discussions throughout preparation.

Competing interests

No competing interests declared

Funding

This work was supported by the Medical Research Council [MR/R022240/2] and a University of Brighton Rising Star Award, both to KS. CF was supported by the Biotechnology and Biological Sciences Research Council (BBSRC) via an Institute Strategic Programme Grant (BB/J004316/1).

Data availability

Data are available upon reasonable request to the corresponding author.

Author contributions

Conception and design of the study: KAS, CF, HJS. Acquisition of data: HJS, KAS, CH, LCL. Drafting the manuscript: HJS, KAS. Revising the manuscript and final approval, and agreement to be accountable for all aspects of the work: all authors.

References

Aigner, T., Zhu, Y., Chansky, H. H., Matsen, F. A., Maloney, W. J. and Sandell, L. J. (1999). Reexpression of type IIA procollagen by adult articular chondrocytes in osteoarthritic cartilage. *Arthritis and Rheumatism* **42**, 1443–1450.

Aspden, R. M. and Saunders, F. R. (2019). Osteoarthritis as an organ disease: From the cradle to the grave. *European Cells and Materials* **37**, 74–87.

Baird, D. A., Paternoster, L., Gregory, J. S., Faber, B. G., Saunders, F. R., Giuraniuc, C. V., Barr, R. J., Lawlor, D. A., Aspden, R. M. and Tobias, J. H. (2018). Investigation of the Relationship Between Susceptibility Loci for Hip Osteoarthritis and Dual X-Ray Absorptiometry–Derived Hip Shape in a Population-Based Cohort of Perimenopausal Women. *Arthritis and Rheumatology* **70**, 1984–1993.

Baird, D. A., Evans, D. S., Kamanu, F. K., Gregory, J. S., Saunders, F. R., Giuraniuc, C. V., Barr, R. J., Aspden, R. M., Jenkins, D., Kiel, D. P., et al. (2019). Identification of Novel Loci Associated With Hip Shape: A Meta-Analysis of Genomewide Association Studies. *Journal of Bone and Mineral Research* **34**, 241–251.

Chang, S. H., Mori, D., Kobayashi, H., Mori, Y., Nakamoto, H., Okada, K., Taniguchi, Y., Sugita, S., Yano, F., Chung, U. il, et al. (2019). Excessive mechanical loading promotes osteoarthritis through the gremlin-1–NF-κB pathway. *Nature Communications* **10**, 1–5.

Cramer, A., De Lima Oliveira, B. C., Leite, P. G., Rodrigues, D. H., Brant, F., Esper, L., Pimentel, P. M. O., Rezende, R. M., Rachid, M. A., Teixeira, A. L., et al. (2019). Role of SOCS2 in the Regulation of Immune Response and Development of the Experimental Autoimmune Encephalomyelitis. *Mediators of Inflammation* **2019**,.

de Andres, M. C., Imagawa, K., Hashimoto, K., Gonzalez, A., Goldring, M. B., Roach, H. I. and Oreffo, R. O. C. (2011). Suppressors of cytokine signalling (SOCS) are reduced in osteoarthritis. *Biochemical and Biophysical Research Communications* **407**, 54–59.

Denko, B. Y. C. W., Boja, B. and Moskowitz, R. W. (1996). Growth factors, insulin-like growth factor-1 and growth hormone, in synovial fluid and serum of patient swith rheumatic disorders. 245–249.

Dobie, R., MacRae, V. E., Pass, C., E.M., M., S.F., A. and C., F. (2018). Suppressor of cytokine signaling 2 (Socs2) deletion protects bone health of mice with DSS-induced inflammatory bowel disease. *DMM Disease Models and Mechanisms* **11**,.

Echtermeyer, F., Bertrand, J., Dreier, R., Meinecke, I., Neugebauer, K., Fuerst, M., Lee, Y. J., Song, Y. W., Herzog, C., Theilmeier, G., et al. (2009). Syndecan-4 regulates ADAMTS-5 activation and cartilage breakdown in osteoarthritis. *Nature Medicine* **15**, 1072–1076.

Ekenstedt, K. J., Sonntag, W. E., Loeser, R. F., Lindgren, B. R. and Carlson, C. S. (2006). Effects of chronic growth hormone and insulin-like growth factor 1 deficiency on osteoarthritis severity in rat knee joints. *Arthritis and Rheumatism* **54**, 3850–3858.

Glasson, S. S., Askew, R., Sheppard, B., Carito, B., Blanchet, T., Ma, H. L., Flannery, C. R., Peluso, D., Kanki, K., Yang, Z., et al. (2005). Deletion of active ADAMTS5 prevents cartilage degradation in a murine model of osteoarthritis. *Nature* **434**, 644–648.

Glasson, S. S., Chambers, M. G., Van Den Berg, W. B. and Little, C. B. (2010). The OARSI histopathology initiative – recommendations for histological assessments of osteoarthritis in the mouse. *Osteoarthritis and Cartilage* **18**, S17–S23.

Keating, N. and Nicholson, S. E. (2019). SOCS-mediated immunomodulation of natural killer cells. *Cytokine* **118**, 64–70.

Kronenberg, H. M. (2003). Developmental regulation of the growth plate. *Nature* **423**, 332–336.

Letellier, E. and Haan, S. (2016). SOCS2□: physiological and pathological functions 3 . BIOLOGICAL FUNCTIONS OF SOCS2. *Frontiers in Bioscience* 189–204.

Lorentzon, M., Greenhalgh, C. J., Mohan, S., Alexander, W. S. and Ohlsson, C. (2005). Reduced bone mineral density in SOCS-2-deficient mice. *Pediatric Research* **57**, 223–226.

Macrae, V. E., Horvat, S., Pells, S. C., Dale, H., Collinson, R. S., Pitsillides, A. A., Ahmed, S. F. and Farquharson, C. (2009). Increased bone mass, altered trabecular architecture and modified growth plate organization in the growing skeleton of SOCS2 deficient mice. *Journal of Cellular Physiology* **218**, 276–284.

Madi, K., Staines, K. A., Bay, B. K., Javaheri, B., Geng, H., Bodey, A. J., Cartmell, S., Pitsillides, A. A. and Lee, P. D. (2019). In situ characterization of nanoscale strains in loaded whole joints via synchrotron X-ray tomography. *Nature Biomedical Engineering* **4**, 343–354.

Metcalf, D., Greenhalgh, C. J., Viney, E., Wilison, T. A., Starr, R., Nicola, N. A., Hilton, D. J. and Alexander, W. S. (2000). Gigantism in mice lacking suppressor of cytokine signalling-2. *Nature* **405**, 1069–1073.

Nagao, M., Hamilton, J. L., Kc, R., Berendsen, A. D., Duan, X., Cheong, C. W., Li, X., Im, H. J. and Olsen, B. R. (2017). Vascular Endothelial Growth Factor in Cartilage Development and Osteoarthritis. *Scientific Reports* **7**, 1–16.

Nagira, K., Ikuta, Y., Shinohara, M., Sanada, Y., Omoto, T., Kanaya, H., Nakasa, T., Ishikawa, M., Adachi, N., Miyaki, S., et al. (2020). Histological scoring system for subchondral bone changes in murine models of joint aging and osteoarthritis. *Scientific Reports* **10**, 10077.

Parfitt, A. M. (2002). Misconceptions (1): Epiphyseal fusion causes cessation of growth. *Bone* **30**, 337–339.

Pass, C., MacRae, V. E., Ahmed, S. F. and Farquharson, C. (2009). Inflammatory cytokines and the GH/IGF-I axis: Novel actions on bone growth. *Cell Biochemistry and Function* **27**, 119–127.

Pass, C., MacRae, V. E., Huesa, C., Faisal Ahmed, S. and Farquharson, C. (2012). SOCS2 is the critical regulator of GH action in murine growth plate chondrogenesis. *Journal of Bone and Mineral Research* **27**, 1055–1066.

Pitsillides, A. A. and Beier, F. (2011). Cartilage biology in osteoarthritis - Lessons from developmental biology. *Nature Reviews Rheumatology* **7**, 654–663.

Saito, T., Fukai, A., Mabuchi, A., Ikeda, T., Yano, F., Ohba, S., Nishida, N., Akune, T., Yoshimura, N., Nakagawa, T., et al. (2010). Transcriptional regulation of endochondral ossification by HIF-2α during skeletal growth and osteoarthritis development. *Nature Medicine* **16**, 678–686.

Samvelyan, H. J., Hughes, D., Stevens, C. and Staines, K. A. (2020). Models of Osteoarthritis: Relevance and New Insights. *Calcified Tissue International*.

Staines, K. A., Madi, K., Mirczuk, S. M., Parker, S., Burleigh, A., Poulet, B., Hopkinson, M., Bodey, A. J., Fowkes, R. C., Farquharson, C., et al. (2016). Endochondral Growth Defect and Deployment of Transient Chondrocyte Behaviors Underlie Osteoarthritis Onset in a Natural Murine Model. *Arthritis and Rheumatology* **68**, 880–891.

Staines, K. A., Madi, K., Javaheri, B., Lee, P. D. and Pitsillides, A. A. (2018). A computed microtomography method for understanding epiphyseal growth plate fusion. *Frontiers in Materials* **4**,.

Staines, K. A., Hardy, R. J., Samvelyan, H. J., Ward, K. A. and Cooper, R. (2020). Life course longitudinal growth and risk of knee osteoarthritis at age 53 years: evidence from the 1946 British birth cohort study.

Wang, M., Sampson, E. R., Jin, H., Li, J., Ke, Q. H., Im, H. J. and Chen, D. (2013). MMP13 is a critical target gene during the progression of osteoarthritis. *Arthritis Research and Therapy* **15**, 1–11.

Xian, C. J., Zhou, F. H., McCarty, R. C. and Foster, B. K. (2004). Intramembranous ossification mechanism for bone bridge formation at the growth plate cartilage injury site. *Journal of Orthopaedic Research* **22**, 417–426.

Figure 1. Socs2 deficient mice exhibit accelerated growth plate fusion mechanisms. (A) Location and areal densities of bridges across the growth plate projected on the medial (M) and lateral (L) tibial joint surface in WT and Socs2$^{-/-}$ (KO) DMM and sham operated joints. **(B)** Number of bridges. **(C)** Areal density (d) of bridges defined as the number of bridges per 256 mm x 256 mm window. **(D)** Location and areal densities of bridges across the growth plate projected on the medial (M) and lateral (L) tibial joint surface in aged WT and Socs2$^{-/-}$ (KO) mice. **(E)** Number of bridges **(F)** Areal density (d) of bridges defined as the number of bridges per 256 mm x 256 mm window. Data are presented as mean ± SEM and showing individual animals. Statistical test performed: Two-way ANOVA with Bonferroni adjustments for multiple comparisons within each joint compartment. * p<0.05 ** p<0.01 *** p<0.001

Figure 2. Deletion of Socs2 does not prevent osteoarthritic articular cartilage lesions in a surgical model of osteoarthritis. (A) Toluidine blue stained sections of the knee joint of WT and Socs2$^{-/-}$ (KO) mice showing development of articular cartilage lesions in the medial tibia. **(B)** Osteophyte severity score **(C)** Mean articular cartilage damage OARSI score and **(D)** Maximum articular cartilage damage OARSI score in WT sham (n = 3), WT DMM (n = 6), KO sham (n = 6) and KO DMM (n = 6). Scale bar = 0.05mm. Data are presented as mean ± SEM and showing individual animals. Statistical test performed: Kruskal-Wallis one-way ANOVA.

Figure 3. Socs2 deficient mice exhibit decreased subchondral bone plate and trabecular number, irrespective of DMM surgically induced osteoarthritis. Micro-CT analysis of the

medial and lateral tibial **(A)** Subchondral bone plate (SCB) thickness (mm) **(B)** SCB bone volume/tissue volume (BV/TV; %) **(C)** Epiphyseal trabecular BV/TV (%) **(D)** Epiphyseal trabecular number (mm^{-1}) **(E)** Epiphyseal trabecular thickness (mm) **(F)** Epiphyseal trabecular separation (mm) in WT and $Socs2^{-/-}$ (KO) mice with DMM or sham surgery (n=6/group). Data are presented as mean ± SEM and showing individual animal data. Statistical test performed: Two-way ANOVA with Bonferroni adjustments for multiple comparisons. *P<0.05; ***P<0.001.

Figure 4. Deletion of Socs2 does not prevent osteoarthritic articular cartilage lesions with ageing. (A) Toluidine blue stained sections of the knee joint of WT and $Socs2^{-/-}$ (KO) mice showing development of articular cartilage lesions in the medial tibia. **(B)** Mean articular cartilage damage OARSI score across the knee joint and **(C)** Maximum articular cartilage damage OARSI score between WT (n=5) and KO (n=6) mice with ageing, in the medial tibia of the knee joint. Scale bar = 0.05mm. Data are presented as mean ± SEM and showing individual animal data. Statistical test performed: Mann-Whitney U test.

Figure 5. Aged Socs2 deficient mice exhibit decreased subchondral bone plate thickness. Micro-CT analysis of the medial and lateral tibial **(A)** Subchondral bone plate (SCB) thickness (mm) **(B)** SCB bone volume/tissue volume (BV/TV; %) **(C)** Epiphyseal trabecular BV/TV (%) **(D)** Epiphyseal trabecular number (mm^{-1}) **(E)** Epiphyseal trabecular thickness (mm) **(F)** Epiphyseal trabecular separation (mm) in aged WT and $Socs2^{-/-}$ (KO) mice (n=6/group). Data are presented as mean ± SEM and showing individual animals. Statistical test performed: Two-way ANOVA with Bonferroni adjustments for multiple comparisons. *P<0.05; ***P<0.001.

Table 1: Weights of wild type (WT) and $Socs2^{-/-}$ (KO) mice during 8-week post-DMM experimental timeline.

	Weight (g)

Week	0	1	2	3	4	5	6	7	8
WT sham	23.2 ± 0.4	22.2 ± 1.0	24.0 ± 0.4	25.6 ± 0.5	26.4 ± 0.7	27.0 ± 0.7	27.6 ± 0.8	28.2 ± 0.8	29.0 ± 0.7
WT DMM	22.4 ± 0.3	21.8 ± 0.3	23.0 ± 0.3	24.0 ± 0.4	24.5 ± 0.3	24.9 ± 0.3	25.6 ± 0.4	25.7 ± 0.3	26.5 ± 0.3
KO sham	32.3 ± 1.2	33.6 ± 0.9	34.8 ± 1.1	35.0 ± 1.0	36.4 ± 1.1	38.1 ± 1.3	38.7 ± 0.9	39.0 ± 0.9	40.4 ± 0.9
KO DMM	31.3 ± 0.8	33.0 ± 0.7	33.7 ± 0.7	34.9 ± 1.0	35.8 ± 1.0	39.8 ± 0.6	38.3 ± 1.1	38.9 ± 1.1	40.3 ± 1.0

424

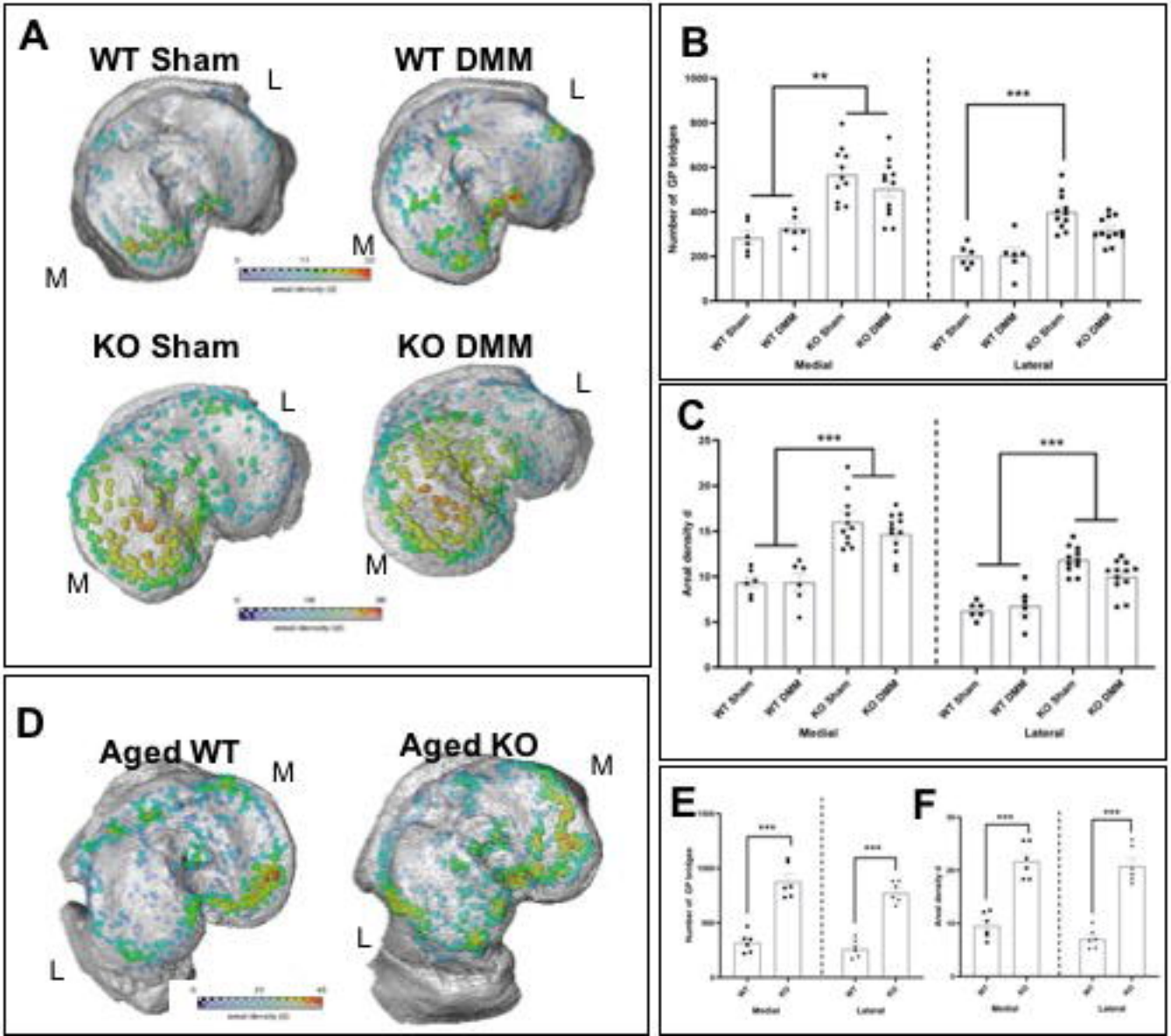
A
WT Sham
WT DMM
KO Sham
KO DMM
L
M
B
Number of GP bridges
**
***
WT Sham
WT DMM
KO Sham
KO DMM
Medial
Lateral
C
Areal density d
***
***
WT Sham
WT DMM
KO Sham
KO DMM
Medial
Lateral
D
Aged WT
Aged KO
L
M
E
F
***
***
***
***
Medial
Lateral

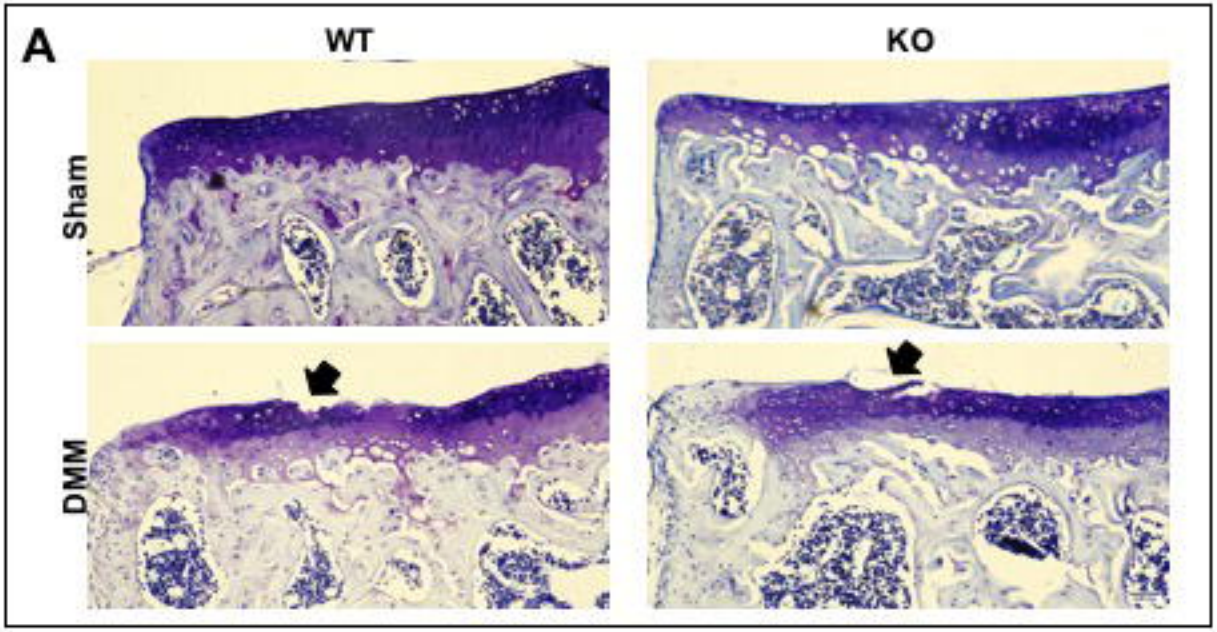
A
WT
KO
Sham
DMM

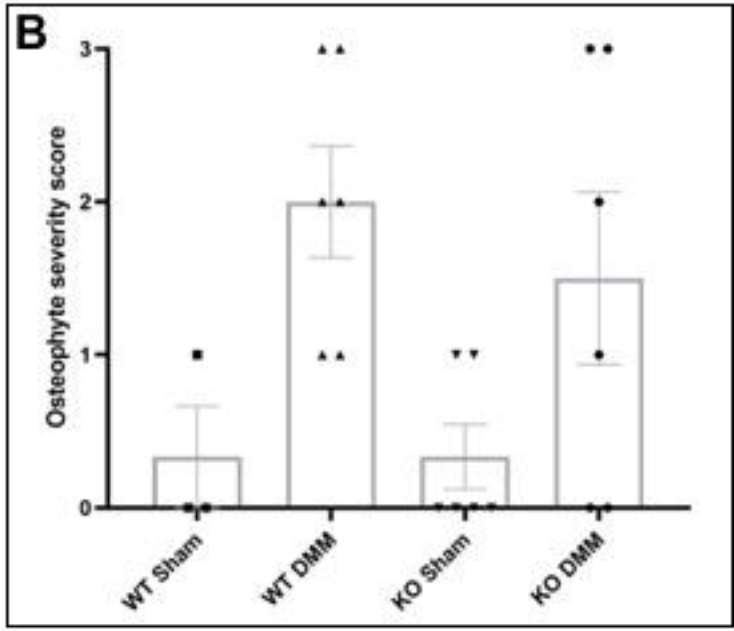
B
Osteophyte severity score
0
1
2
3
WT Sham
WT DMM
KO Sham
KO DMM

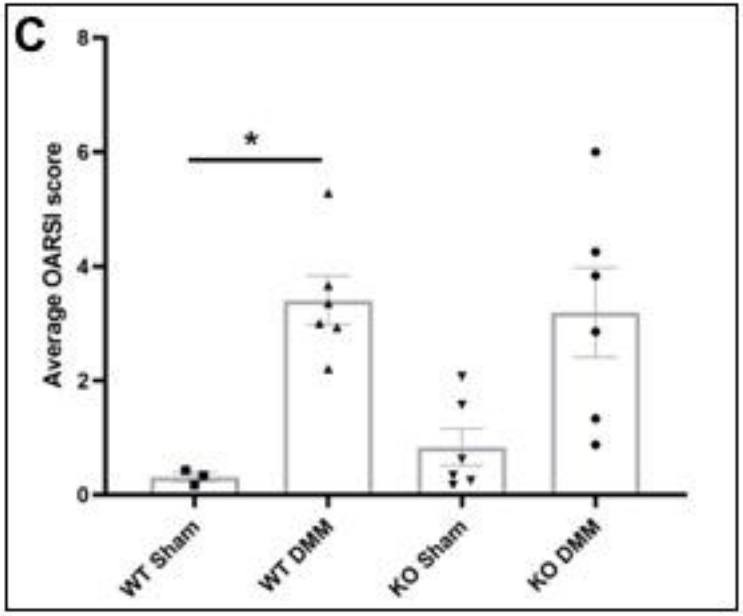
C
Average OARSI score
0
2
4
6
8
*
WT Sham
WT DMM
KO Sham
KO DMM

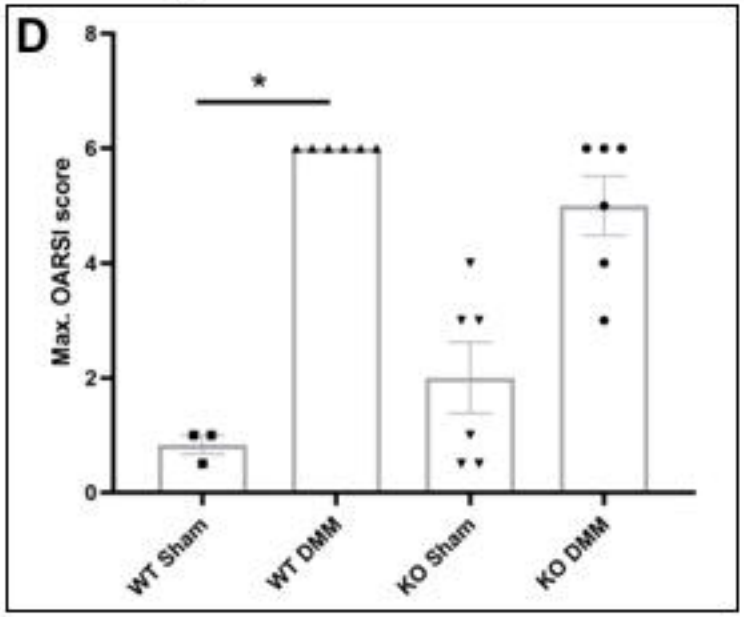
D
Max. OARSI score
0
2
4
6
8
*
WT Sham
WT DMM
KO Sham
KO DMM

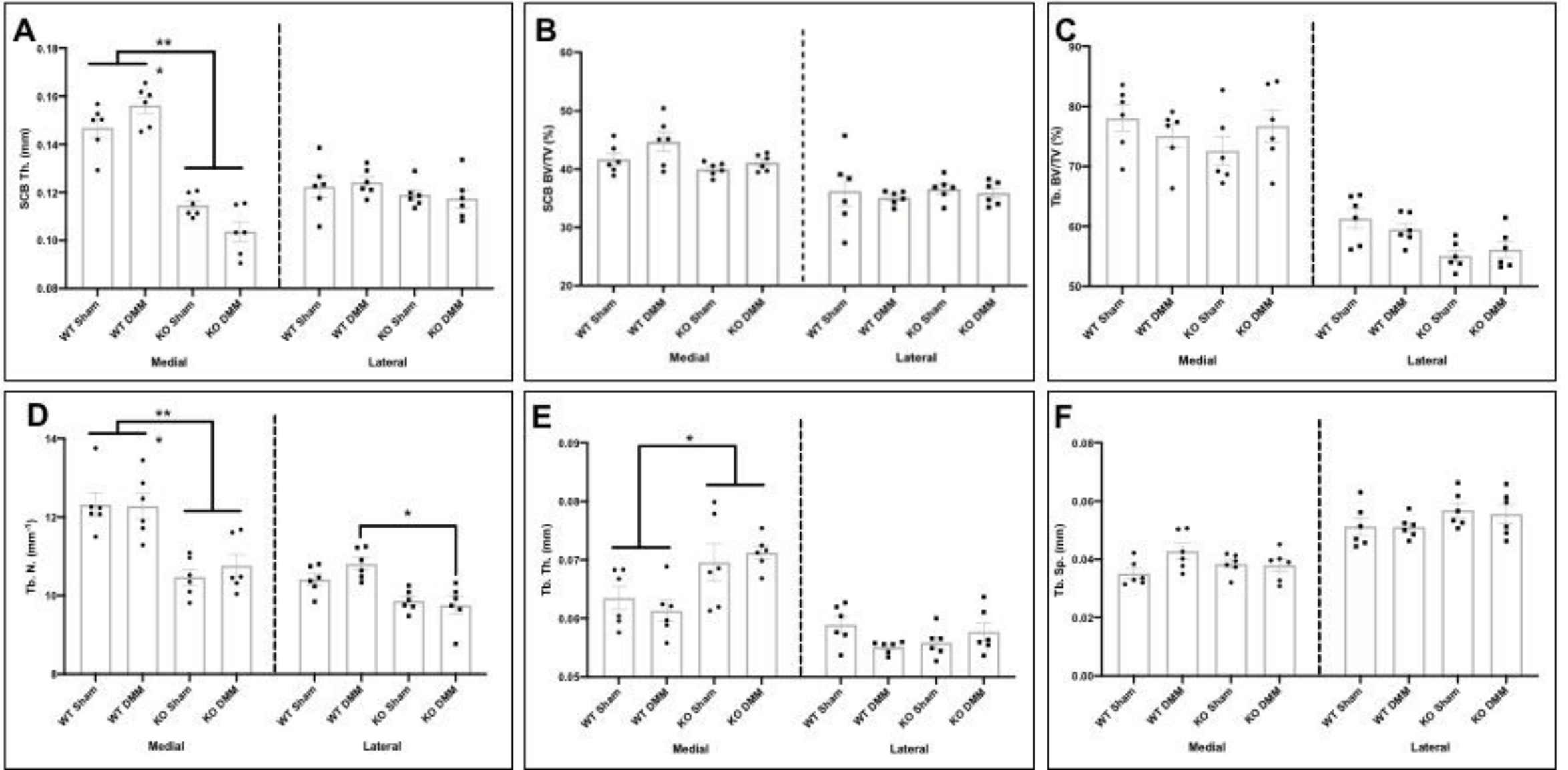
A
SCB Th. (mm)
0.18
0.16
0.14
0.12
0.10
0.08
**
*
WT Sham
WT DMM
KO Sham
KO DMM
Medial
Lateral
B
SCB BV/TV (%)
60
50
40
30
20
C
Tb. BV/TV (%)
90
80
70
60
50
D
Tb. N. (mm⁻¹)
14
12
10
8
E
Tb. Th. (mm)
0.09
0.08
0.07
0.06
0.05
F
Tb. Sp. (mm)
0.08
0.06
0.04
0.02
0.00

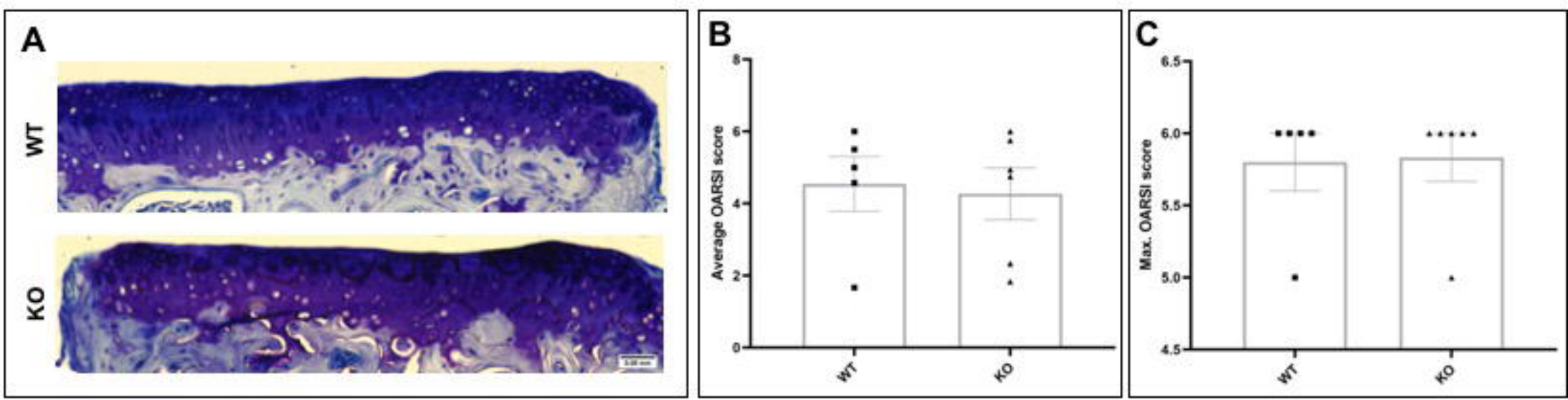
A
WT
KO
B
Average OARSI score
8
6
4
2
0
WT
KO
C
Max. OARSI score
6.5
6.0
5.5
5.0
4.5
WT
KO

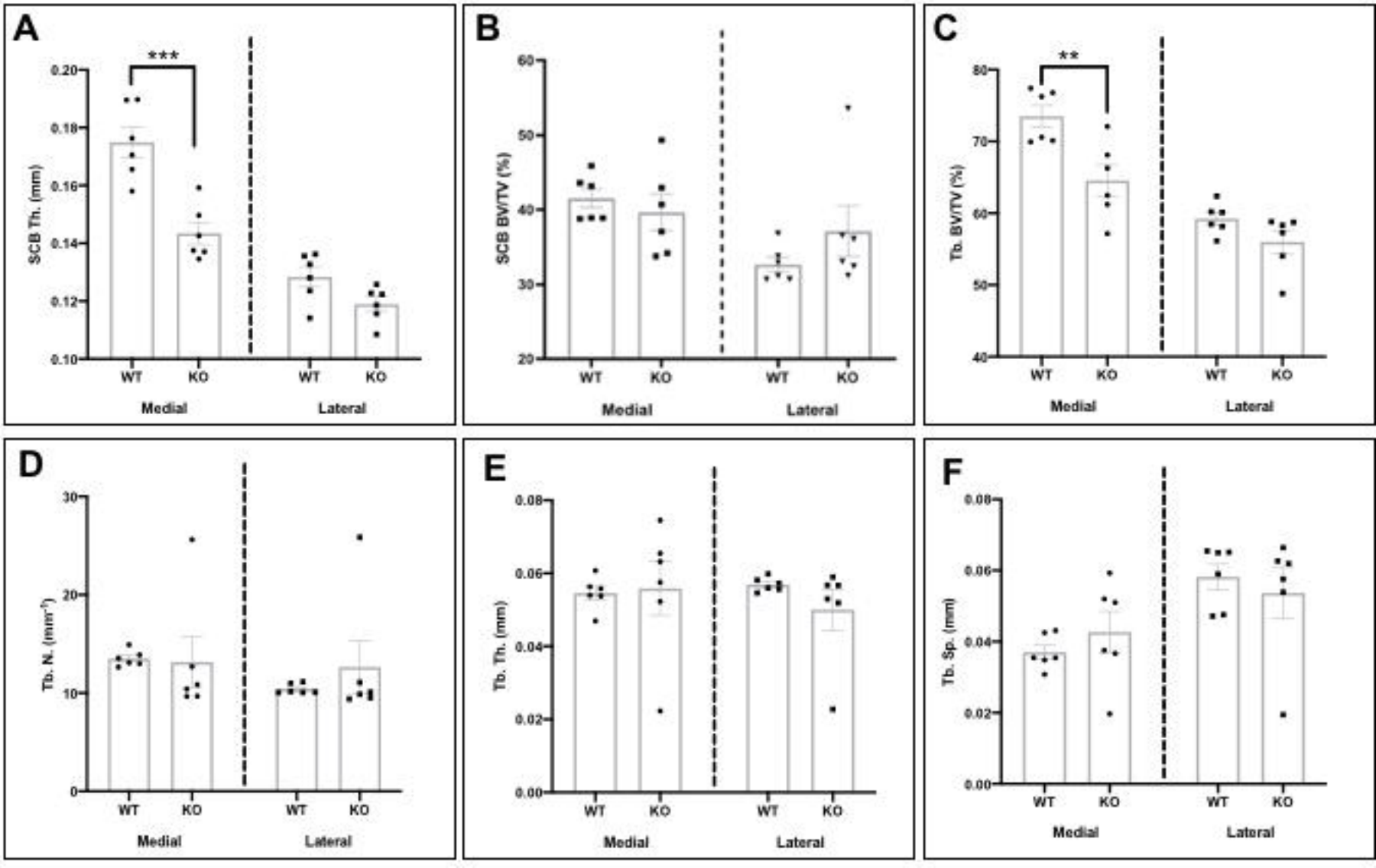
A
***
SCB Th. (mm)
0.20
0.18
0.16
0.14
0.12
0.10
WT
KO
WT
KO
Medial
Lateral
B
SCB BV/TV (%)
60
50
40
30
20
WT
KO
WT
KO
Medial
Lateral
C
**
Tb. BV/TV (%)
80
70
60
50
40
WT
KO
WT
KO
Medial
Lateral
D
Tb. N. (mm⁻¹)
30
20
10
0
WT
KO
WT
KO
Medial
Lateral
E
Tb. Th. (mm)
0.08
0.06
0.04
0.02
0.00
WT
KO
WT
KO
Medial
Lateral
F
Tb. Sp. (mm)
0.08
0.06
0.04
0.02
0.00
WT
KO
WT
KO
Medial
Lateral